RSC Advances

ROYAL SOCIETY OF CHEMISTRY

www.rsc.org/advances

Asymmetric and symmetric solid-state supercapacitors based on 3D interconnected polyaniline-carbon nanotube framework

Mohd. Khalid*, Milton A. Tumelero, Andre A. Pasa*

Abstract

In this work, we demonstrate multiwalled carbon nanotube (MWCNT)-assisted polyaniline (PANI) thin films to improve supercapacitor performance. The thin films of PANI have been potentiostatically deposited onto gold coated PET sheet with the assistance of MWCNT. The assistance of MWCNT results in the formation of unique nanostructured PANI framework which provides better accessibility for supercapacitive behavior. The solid-state supercapacitor has been made using two slightly separated thin films of MWCNT-assisted PANI (MWCNT-PANI) by H_3PO_4-polyvinyl alcohol (H_3PO_4-PVA) gel electrolyte. The asymmetric solid-state supercapacitor (ASS) and symmetric solid-state supercapacitor (SSS) devices exhibit the remarkable area-specific capacitance of 23.1 mF/cm^2 (660 F/cm^3) and 8.3 mF/cm^2 (119 F/cm^3), respectively. The ASS and SSS devices have the energy density 2.7 mWh/cm^2 and 0.95 mWh/cm^2 while maintaining the power density of 337 mW/cm^2 and 263 mW/cm^2, and excellent cyclic stability. The electrochemical properties of MWCNT-PANI films have also been investigated in aqueous H_2SO_4 and organic tetraethyl ammonium tetrafluoroborate electrolytes in half cell configuration.

Introduction

The increasing demand for lightweight and small form of the portable devices having high power, high energy, and long cycle life have stimulated intense research on energy storage devices. Among the energy storage systems supercapacitors are considered to be one of the most important modern innovations for electrical energy storage. Particularly great attention has been focused on the development of flexible supercapacitor [1]. Based on the charge storage mechanism, supercapacitors can be divided into electrochemical double layer capacitors and pseudocapacitors, in which energies are stored in the form of electric double layer at the interface of electrode/electrolyte, and reversible redox reactions (pseudocapacitance) of the electroactive species, respectively.

Conductive carbon based materials are usually adopted as electrode materials for storing the charge through electrochemical double layer and can exhibit high power densities, because faster ion flow than redox reactions. On the other hand, conducting polymers and metal oxides are usually used as pseudocapacitors electrode materials, which store energy through redox reactions and can exhibit high energy densities. Among the conducting polymers, PANI (polyaniline) is regarded as one of the most promising materials due to its excellent conductivity, high electrochemical activity, stability in air and water, low cost, and ease of synthesis [2-6]. However, PANI often suffer from poor cyclic stability as electrode materials for supercapacitors because of swelling and shrinking of the material during charge-discharge process [7]. To improve the electrochemical performance of PANI-based electrodes considerable research efforts have been placed on exploring hybrid composite structures where PANI is combined with carbon materials, which enable large area, chemical stability, and low cost electrode material to be constructed. Since past decade several methodologies have been developed to integrate carbon nanotubes and PANI such as stirring [8-11], static placement [12], sonication [13-17], and emulsion polymerization [18-22]. Despite the all procedures reported, the electrodeposited thin film of PANI as flexible supercapacitor has met with very limited success.

Recently, we have demonstrated the codeposition of PANI nanofibers and graphene oxide nanoplatelet composite thin films [23]. The resulting electrodeposited nanocomposite films exhibited excellent supercapacitive performance due to the unique structure of the materials which provide the synergistic combination between PANI nanofibers and graphene oxide nanoplatelets. Currently, aqueous and organic electrolytes have been widely utilized for electrochemical capacitors [24-26]. Due to the low voltage window of aqueous electrolyte based supercapacitor than organic electrolyte based supercapacitor they have lower energy density [24,27]. However, for organic electrolytes the flammability, toxicity, and environmentally hazardous nature are the main drawbacks. While liquid electrolyte-based supercapacitors requires high-standard safety once they become leakage it harms our living environment and the components part of the configuration are not an integrate one, which reduce the electrochemical performance under device movement. Solid-state supercapacitors have certain advantages over liquid electrolyte-based supercapacitors such as lightweight, good flexibility, high safety and environmental stability, which are important for portable devices. The problems, as mentioned above, can be partially avoided by using gel polymer electrolyte instead of aqueous and organic electrolytes.

Over the past few years, some efforts have been done in the development of solid-state devices based on PANI and CNTs [28-30], the fabrication of solid-state devices from thin, lightweight, flexible and freestanding films of MWCNT-assisted PANI have not yet been reported extensively. The present work reports the electrodeposition of PANI in the presence of MWCNTs onto gold coated PET sheet by using a simple one-step electropolymerization method. Gold coated PET sheet was used as a current collector, leading to a simple flexible and lightweight architecture. The deposited thin film electrodes were employed in H_3PO_4-PVA polymer gel electrolyte in solid-state two-electrode cell configuration and the electrochemical properties of the film electrodes were also analyzed in three-electrode cell configuration by using aqueous H_2SO_4, and organic tetraethyl ammonium tetrafluoroborate ($TEABF_4$) electrolytes.

Experimental Methods

The MWCNTs were synthesized using CVD method by the Group of Nanomaterials at the Federal University of Minas Gerais, Brazil. MWCNTs were several micrometers in length and have more than 95% purity. Following a reported procedure [31], MWCNTs were treated with 3:1 mixture of concentration of H_2SO_4 and HNO_3 acids under ultrasonic bath for 3 h at 50^oC to introduce carboxylic acids on the surface of MWCNTs. Upon completion, the mixture was added drop wise to 300 mL cold de-ionized water and then filtered through centrifugation (6000 rpm for 20 min). The residual was then dried in oven at 60°C for 24 h. The stable dispersion of MWCNTs in water (1.2 mg mL^{-1}) was prepared then used in electrochemical polymerization of PANI thin film. MWCNTs were added in 50 mL of 0.12 mol L^{-1} aniline solution (made in 1 mol L^{-1} H_2SO_4) and stirred for 10 min to form a uniform dispersion before electropolymerization. Different contents of MWCNTs dispersion such as 0.05, 0.1, 0.2, and 0.3 mL were employed and the obtained films were labeled as MWCNT-PANI-a, MWCNT-PANI-b, MWCNT-PANI-c, and MWCNT-PANI-d, respectively.

Electrodeposition was carried out in a one-compartment three electrodes connected cell using a potentiostat (Autolab PGSTAT 302N) electrochemical workstation at room temperature (25°C) under computer control. In which the counter electrode was platinum, the reference electrode was saturated calomel electrode (SCE), and a layer of gold about 50 nm thick was deposited onto the poly(ethylene terephthalate) (PET) sheet by using e-beam evaporator, this gold film was adopted as working electrode. The all electrochemical deposition processes were carried out at a constant applied oxidative potential of 700 mV *vs.* SHE for 700 sec. The electrodeposited films were washed gently with de-ionized water, dried under flowing nitrogen and stored in vacuum desiccators for several hours. For comparison, a pure PANI film was also synthesized electrochemically in the absence of MWCNTs *via* similar procedure described above. The galvanostatic charge-discharge tests were measured with different voltage windows for different electrolytes: 1 V for 1 mol L^{-1} $TEABF_4$, 0.7 for 1mol L^{-1} H_2SO_4, and 0.5 V for H_3PO_4-PVA polymer gel electrolyte. The specific capacitance (C_s) of an electrode in three-electrode measurements, as a function of current densities, was calculated from discharge curves by applying the equation:

$$\mathrm{C_s} = \frac{\mathrm{I}}{A\,(\frac{dV}{dt})}$$

where I is the discharge current in amperes, A is the area (cm^2) of active material on the substrate, and dt is the discharge time (sec) corresponding to the voltage difference dV in volts. dV/dt can be obtained from the slope of the discharge curve.

The proton conducting gel polymer electrolyte was synthesized using the solution casting process according to a previously reported method [32, 37]. In brief, PVA (molecular weight 89,000-98,000, 99% hydrolyzed, Sigma-Aldrich) powder was mixed with water (1 g PVA/10 g H_2O). The mixture was heated at ~ 90 °C under constant stirring until the solution turned clear. After cooling under ambient conditions, 0.8 g of concentrated phosphoric acid (H_3PO_4) solution (85% solution in water, Sigma-Aldrich) was added and the solution was stirred thoroughly. PVA acts as a kind of glue and host for ionic conduction. The ion source comes from H_3PO_4 as a proton donor acid. A 1mol L^{-1} H_2SO_4 was prepared in de-ionized water, and 1 mol L^{-1} $TEABF_4$ was prepared by adding $TEABF_4$ salt in anhydrous acetonitrile. All the chemicals used in these experiments were of analytical grade (Sigma-Aldrich) and without further purification. The solutions were prepared using Milli-Q grade water (18.2 MΩ.cm).

Scanning electron microscopy (SEM; JEOL JSM-6390LV) at 15 kV was used to observe the morphology of the materials. The samples were coated with gold before their observation. The UV-visible spectra of the materials were recorded at ambient temperature from 200 to 900 nm wavelength using a Perkin Elmer 750 spectrophotometer. The solutions used for the measuring the absorption spectra of PANI, MWCNT-PANI, and MWCNT were prepared by dispersing the samples in isopropyl alcohol.

Results and discussion

The solid-state supercapacitor devices were assembled in a sandwich style. The fabrication process is illustrated in Fig. 1a. The device was assembled by pouring polymer gel electrolyte slowly onto the film electrodes before sandwiching the two electrodes. This assembly was left under ambient conditions for 2 h to allow the evaporation of excess water. The two thin film electrodes were then pressed gently and left overnight. The polymer gel acts as both electrolyte and ion porous separator as well as provides the mechanical integrity to the assembly. This assembly was wrapped with Kapton tape. The active surface area of each thin film electrode was made assessable 1.5 cm^2. Here the MWCNT-PANI film is used as active material and gold coated PET sheet serves as a current collector. The resulting device was mechanically robust and flexible. The SSS device was assembled by using two MWCNT-PANI films (same material and format for both electrodes) and the ASS device was assembled based on MWCNT-PANI film as positive electrode and copper coated PET sheet as negative electrode with polymer gel electrolyte separator. In comparison with the liquid electrolyte-based supercapacitors, solid-state supercapacitors have certain advantages such as lightweight, good flexibility, high safety and environmentally benign nature. The success of electropolymerization is demonstrated in digital image of Fig. 1b, which clearly shows a shiny green color coating of material on the surface of the substrate.

The morphology of PANI film is different when electrodeposited in the presence of MWCNTs. According to the SEM images (Fig. 2), instead of formation of a smooth surface as in case of pure PANI film (Fig. 2b), the existence of MWCNT results in the formation of triangular cross-linked network microstructures (Fig. 2c) on the surface of the substrate. It is believed that the presence of MWCNT in the electrolyte during electrodeposition induces different pathway for the growth electroactive PANI films and increase the specific surface area. The observable fact of this mechanism is still vogue but apparently the presence of MWCNT is responsible for the triangular cross-linked network microstructures of PANI. Fig. 2d shows the cross section view of two separated electrodes with polymer gel electrolyte thickness is about ~ 50 µm. Fig. 2e shows the profilometer measurement indicating a thickness about 350 nm for MWCNT-PANI electrodes. The thickness was used to calculate the volumetric-specific capacitance. The UV-vis spectrum of the MWCNT-PANI composite in Fig. 3 displays essentially the same absorption characteristics as that of pure PANI. The peaks at 345, 450 and 800 nm are attributed to the emeraldine salt form of PANI [33-35]. The UV-vis spectrum of the MWCNTs in isopropyl alcohol solution shows the peak at 260 nm and decreases from UV to near IR.

Supercapacitor performance

The electrochemical performance of MWCNT-PANI films was evaluated by cyclic voltammetric (CV) and galvanostatic charge-discharge measurements. On the basis of the high capacitance measured for sample MWCNT-PANI-c in the $TEABF_4$ electrolyte shown in Table 1, it was selected for the construction of ASS and SSS devices. Fig. 4a presents the CV curves of MWCNT-PANI-c with H_2SO_4, $TEABF_4$, and H_3PO_4-PVA electrolytes. In comparison of aqueous H_2SO_4, the organic $TEABF_4$ and polymer gel H_3PO_4-PVA electrolytes demonstrate the relatively rectangular shape of CV for MWCNT-PANI electrode at the scan rate of 200 mV/s in the potential window range -0.2 to 0.9 V. The small reversible humps were observed in the CV of MWCNT-PANI-c with H_3PO_4-PVA and $TEABF_4$ electrolytes at various scan rates of 10 to 200 mV/s (Fig. 4b & c); these reversible humps derived from different oxidation states of PANI. However, the linear profile and triangular shape of galvanostatic charge and discharge curves of MWCNT-PANI-c with $TEABF_4$ and H_3PO_4-PVA electrolytes, affirming the typical electrostatic double layer capacitance as shown in Fig. 5a & b. This feature has been associated to the very little contribution of pseudocapacitance and the total capacitance is mainly achieved by electric double layer in H_3PO_4-PVA and $TEABF_4$ electrolytes.

The specific capacitance of MWCNT-PANI thin film electrodes in organic $TEABF_4$ electrolyte increases as increasing the contents of MWCNT in electrolyte solution during electrodeposition of PANI. When the MWCNT contents increase to 2 mL (1.2 mg/mL dispersion of MWCNT in water), the specific capacitance of MWCNT-PANI-c film reaches its maximum (85.8 mF/cm^2). Thereafter, the specific capacitance decreases with the increasing MWCNT contents (Table 1). Fig. 5a demonstrates the galvanostatic charge-discharge curves of pure PANI and

MWCNT-PANI-c in $TEABF_4$ electrolyte. The MWCNT-PANI-c exhibited longer charge-discharge time than pure PANI thin film electrode and their calculated specific capacitances are shown in Table 1. Fig. 5b shows the area-specific capacitances of ASS and SSS devices were calculated using galvanostatic discharge curves to be 22.3 mF/cm^2 (637 F/cm^3) and 7.8 mF/cm^2 (111 F/cm^3) at 0.5 mA applied current, respectively. To better comparison of the specific capacitance with previous CNT/PANI reports, we presumed a mass density of 0.8 g/cm^3 according to our previous reported work [23]. The gravimetric capacitance of 510 F/g for half-cell electrode and 89 F/g for solid-state supercapacitor (SSS) were calculated. These values are fairly high than those reported in ref [28-29].

Further we measured the area-specific capacitance of MWCNT-PANI-c electrode with different electrolytes at three different applied currents (0.1, 0.5, and 1 mA) as shown in Fig 6. The MWCNT-PANI-c electrode exhibited high capacitance with organic $TEABF_4$ electrolyte compared to aqueous H_2SO_4 and polymer gel H_3PO_4-PVA electrolytes. MWCNT-PANI thin film electrode showed higher operating voltage window (1 V) for $TEABF_4$ electrolyte compared to H_2SO_4 and H_3PO_4-PVA electrolytes. The organic electrolyte-based supercapacitors have relatively large electrochemical windows than aqueous electrolyte because of thermodynamic decomposition potential of water which constricts the operating voltage window [1, 24, 27]. The solid- state supercapacitor devices showed lower capacitance than aqueous and organic electrolytes. This may be because of the slower ions mobility in the polymer gel electrolyte. Even though, the area-specific capacitance of solid-state supercapacitors is quite comparable and exceeded than some capacitance values reported as based on graphene quantum dots thin film microsupercapacitor (0.53 mF/cm^2) [36], laser scribing graphene supercapacitor in gel polymer electrolyte (2.32 mF/cm^2) [37], RGO film with gel polymer electrolyte (0.0807 mF/cm^2) [38], hydrated GO film by laser scribing in excess of water (0.51 mF/cm^2) [39], ZnO nanowires/graphene films (0.4 mF/cm^2) [40,41], graphene/Au wire (ca. 0.7 mF/cm^2) [42], the electrochemical micro-supercapacitors (0.4-2 mF/cm^2), GF@3D-G supercapacitors (1.2-1.7 mF/cm^2) [43], graphene based paper supercapacitor (2.3 mF/cm^2) [44], thermally exfoliated graphene (12.4 μF/cm^2) [45], graphene-based in-plane micro-supercapacitor (80.7 μF/cm^2) [46], micrometre-sized supercapacitors based on onion-like carbon (1.7 μF/cm^2) [47], and carbon nanotube-nanocup hybrid structure (0.6 mF/cm^2) [48]. Further, we believe that the capacitive performance of MWCNT-PANI can be much more improved by reducing the thickness of the gel electrolyte between two-electrodes as recently demonstrated [28,49,50].

For practical applications, cyclic stability is a crucial factor. To characterize the cyclic stability of ASS and SSS devices, galvanostatic charge-discharge tests were carried out up to 1000 cycles as shown in Fig. 7. Remarkably, only 9% decay in specific capacitance for SSS device and 20% decay in specific capacitance for ASS devices were observed. SSS device shows excellent cyclic stability and >91% of the initial specific capacitance was retained even after 1000 cycles. The discharge curves remained symmetric with charge counterparts and displayed linear voltage time profiles after cycling 1000 times (inset Fig. 7). The voltage drop at the beginning of discharge curves of ASS and SSS devices were observed 0.12 and 0.034 V, respectively (Fig. 5b). The lower voltage drop for SSS may be due to the electrode material which corresponds to the low internal resistance [51]. The solid-state device was tested under mechanical deformation. Fig. 8 depict the galvanostatic charge-discharge curves for SSS device on straight and deformation status demonstrating that the electrochemical behavior was affected under mechanical deformation. This could be due to the disturbance in the proximity between two electrodes under mechanical deformation. The discharge curve was slightly lower shifted from the straight one it means capacitance was decreased under mechanical deformation.

In order to need high voltage and high operating current for practical applications, three ASS devices were assembled both in series and in parallel configurations. Compared with a single device, which operates at 0.5 V potential windows, the three devices connected in series exhibited a 1.5 V charge-discharge potential window with similar discharge time as expected (Fig. 9). In the parallel assembly, the discharge time was about four times of a single device at the same current condition

(0.1 mA) while the operating voltage remains the same (0.5 V), as displayed in Fig. 9. In this case, the expected discharge time is 3 times of a single capacitor and the observed value could be explained by dissimilarity between devices that is more critical for the parallel configuration. As with the single device both series and parallel devices show the triangular charge-discharge curves which indicate the excellent capacitive properties.

Energy density (E) and power density (P) are also used as figures of merit for the capacitors and can be calculated from the equations as given below [52].

$$\mathrm{E} = \frac{1}{2}\mathrm{C_s}V^2$$

$$\mathrm{P} = \frac{\mathrm{E}}{\mathrm{t}}$$

where $\mathrm{C_s}$ is the specific capacitance in mF/cm^2, V is the operating voltage window in Volts, and t is the discharge time in hours. According to the above equations, the area-specific capacitance 21.7 mF/cm^2 of ASS device was corresponding to the energy density of 2.7 mWh/cm^2 at the power density of 337 mW/cm^2. The area-specific capacitance 7.6 mF/cm^2 of SSS device was corresponding to the energy density of 0.95 mWh/cm^2 at the power density of 263 mW/cm^2 at the same applied current of 0.5 mA. These area-specific energy density values are quite resemble than some lately reported results [53-57].

Conclusions

In conclusion, a solid-state supercapacitor based on MWCNT-assisted PANI films were designed and fabricated using a convenient electrochemical polymerization process. The assembled asymmetric and symmetric supercapacitors exhibited high electrochemical performance; including high area-specific capacitance, high volumetric-specific capacitance, excellent cyclic stability, and remarkable energy and power densities. The unique triangular interconnected fibers network structure of the material facilitated the accessibility of enhanced performance of solid-state supercapacitor. In the view of practical applications, we believe that the present method of MWCNT-assisted PANI deposition in the form of thin film provides an efficient and promising way to produce high-performance solid-state supercapacitor applications.

Acknowledgments

This research was funded by Brazilian agencies CAPES, FINEP, CNPQ, and FAPESC. The authors wish to thank A. S. Ferlauto from the Group of Nanomaterials at the Federal University of Minas Gerais, Brazil, for providing MWCNTs.

Notes and references

Laboratório de Filmes Finos e Superfícies, Departamento de Fisica,Universidade Federal de Santa Catarina 88040-900-Florianopolis, Brazil

*Corresponding authors e-mail address: mkansarister@gmail.com (M. Khalid), andre.pasa@ufsc.br (A.A. Pasa). Tel.: +55 4884061547

1 Y. Shao, M. F. El-Kady, L. J. Wang, Q. Zhang, Y. Li, H. Wang, M. F. Mousavi, R. B. Kaner, Chem. Soc. Rev. 2015, **44,** 3639-3665.

2 A. G. Macdiarmid, J. C. Chiang, A.F. Richter, A. J. Epstein, *Synth. Met.,* 1987, **18,** 285-290.

3 J. X. Huang, R. B. Kaner, *J. Am. Chem. Soc.,* 2004, **126,** 851-855.

4 Y. Z. Long, Z. J. Chen, X. T. Zhang, J. Zhang, Z. F. Liu, *Appl. Phys. Lett.,* 2004, **85,** 1796-1798.

5 M. Q. Wu, L. P. Zhang, D. M. Wang, J. H. Gao, S. R. Zhang, *Nanotechnology,* 2007, **7,** 385603-385610.

6 C. Z. Meng, C. H. Liu, S. S. Fan, *Electrochem. Commun*., 2009, **11,** 186-189.

7 D. Belanger, X. M. Ren, J. Davey, F. Uribe, S. Gottesfeld, *J. Electrochem. Soc.,* 2000, **147,** 2923-2929.

8 Q. Yao, L. D. Chen, W. Q. Zhang, S. C. Liufu, X. H. Chen, *ACS Nano,* 2010, **4,** 2445-2451.

9 R. Sainz, W. R. Small, N. A. Young, C. Valles, A. M. Benito, W. K. Maser, M. Panhuis, *Macromolecules,* 2006, **39,** 7324-7332.

10 A. L. Cabezas, Z. B. Zhang, L. R. Zheng, S. L. Zhang, *Synth. Met.,* 2010, 160, 664-668.

11 J. Q. Dong, Q. J. Shen, *Polym. Sci. Part B*, 2009, **47,** 2036-2046.

12 Z. X. Wei, M. X. Wan, T. Lin, L. M. Dai, *Adv. Mater.,* 2003, **15,** 136-139.

13 P. Jimenez, W. K. Maser, P. Castell, M. T. Martínez, A. M. Benito, Macromol. *Rapid Commun.*, 2009, **30,** 418-422.

14 P. Jimenez, P. Castell, R. Sainz, A. Anson, M. T. Martínez, A. M. Benito, W. K. Maser, *J. Phys. Chem. B*, 2010, **114,** 1579-1585.

15 R. Sainz, A. M. Benito, M. T. Martínez, J. F. Galindo, J. Sotres, A. M. Baro, B. Corraze, O. Chauvet, W. K. Maser, *Adv. Mater.*, 2005, **17,** 278-281.

16 F. Yılmaz, Z. Kucukyavuz, *J. Appl. Polym. Sci.*, 2009, **111,** 680-684.

17 M. Ginic-Markovic, J. G. Matisons, R. Cervini, G. P. Simon, P. M. Fredericks, *Chem. Mater.,* 2006, **18,** 6258-6265.

18 T. Jeevananda, K. N. H. Siddaramaiah, S. B. Heo, J. H. Lee, *Adv. Technol.,* 2008, **19,** 1754-1762.

19 D. K. Kim, K. W. Oh, S. H. J. Kim, *Polym. Sci. Part B*, 2008, **46,** 2255-2266.

20 E. Zelikman, R. Y. Suckeveriene, G. Mechrez, M. Narkis, Polym. *Adv. Technol.*, 2010, **21,** 150-152.

21 Z. Niu, P. Luan, Q. Shao, H. Dong, J. Li, J. Chen, D. Zhao, L. Cai, W. Zhou, X. Chen, S. Xie, *Energy Environ. Sci.,* 2012, **5,** 8726-8733.

22 Y. K. Zhou, B. L. He, W. J. Zhou, J. Huang, X. H. Li, B. Wu, H. L. Li, *Electrochim. Acta,* 2004, **49,** 257-262.

23 Mohd. Khalid, M. A. Tumelero, V. C. Zoldan, C. C. Pla Cid, D. F. Franceschini, R. A. Timm, L. T. Kubota, S. A. Moshkalev, A. A. Pasa, *RSC Advances,* 2014, **4,** 34168-34178.

24 B. E. Conway, Electrochemical Supercapacitors: Scientific Fundamentals and Technological Applications, Kluwer Academic Plenum, New York, 1999.

25 R. Kötz, M. Carlen, *Electrochim. Acta,* 2000, **45,** 2483-2498.

26 G. Wang, L. Zhang, J. Zhang, *Chem. Soc. Rev.,* 2012, **41,** 797-828.

27 V. Ruiz, R. Santamaria, M. Granda, C. Blanco, *Electrochim. Acta,* 2009, **54,** 4481-4486.

28 C. Meng, C. Liu, L. Chen, C. Hu, S. Fan, *Nano Lett*., 2010, **10,** 4025-4031.

29 J. Ge, G. Cheng, L. Chen, *Nanoscale*, 2011, **3,** 3084-3088.

30 H. Lin, L. Li, J. Ren, Z. Cai, L. Qiu, Z. Yang, H. Peng, *Sci. Rep.,* 2013, **3,** 1353-1358.

31 J. Liu, A. G. Rinzler, H. Dai, J. H. Hafner, R. K. Bradley, P. J. Boul, A. Lu, T. Iverson, K. Shelimov, C. B. Huffman, F. R. Macias, Y.S. Shon, T. R. Lee, D. T. Colbert, R. E. Smalley, *Science*, 1998, **280,** 1253-1256.

32 M. Kaempgen, C. K. Chan, J. Ma, Y. Cui, G. Gruner, *Nano Lett.*, 2009, **9,** 1872-1876.

33 Y. Liao, C. Zhang, Y. Zhang, V. Strong, J. Tang, X. G. Li, K. K. Zadeh, E. M. V. Hoek, K. L. Wang, R. B. Kaner, *Nano Lett.*, 2011, **11,** 954-959.

34 J. X. Huang, S. Virji, B. H. Weiller, R. B. Kaner, *J. Am. Chem. Soc.,* 2003, **125,** 314-315.

35 J. X. Huang, R. B. Kaner, *J. Am. Chem. Soc.,* 2004, **126,** 851-855.

36 W. Liu, Y. Feng, J. Chen, Q. Xue, Adv. *Funct. Mater.,* 2013, **23,** 4111-4122.

37 M. F. El-Kady, R. B. Kaner, *Nature Commun.*, 2013, **4,** 1475.

38 Z. Wu, K. Parvez, X. Feng, K. Mullen, *Nature Commun.*, 2013, **4,** 2487.

39 W. Gao, N. Singh, L. Song, Z. Liu, A. L. M. Reddy, L. Ci, R. Vajtai, Q. Zhang, B. Wei, P. M. Ajayan, *Nat. Nanotechnol.*, 2011, **6,** 496-500.

40 J. Bae, M. K. Song, Y. J. Park, J. M. Kim, M. Liu, Z. L. Wang, *Angew. Chem.,* 2011, **50,** 1683-1687.

41 J. Bae, Y. J. Park, M. Lee, S. N. Cha, Y. J. Choi, C. S. Lee, J. M. Kim, Z. L. Wang, *Adv. Mater.,* 2011, **23,** 3446-3449.

42 Y. R. Li, K. X. Sheng, W. J. Yuan and G. Q. Shi, *Chem. Commun.* 2013, **49,** 291-293.

43 Y. Meng, Y. Zhao, C. Hu, H. Cheng, Y. Hu, Z. Zhang, L. Qu, *Adv. Mater.*, 2013, **25,** 2326-2331.

44 G. Zheng, L. Hu, H. Wu, X. Xie, Y. Cui, *Energy Environ. Sci.,* 2011, **4,** 3368-3373.

45 S. Vivekchand, C. Rout, K. Subrahmanyam, A. Govindaraj, C. Rao, *J. Chem. Sci.*, 2008, **120,** 9-13.

46 Z. S. Wu, K. Parvez, X. Feng, K. Mullen, *Nature Comm.* 2013, **4,** 2487.

47 D. Pech, M. Brunet, H. Durou, P. Huang, V. Mochalin, Y. Gogotsi, P.L. Taberna, P. Simon, *Nat. Nanotechnol.,* 2010, **5,** 651-654.

48 M. G. Hahm, A. L. M. Reddy, D. P. Cole, M. Rivera, J. A. Vento, J. Nam, H. Y. Jung, Y. L. Kim, N. T. Narayanan, D. P. Hashim, C. Galande, Y. J. Jung, M. Bundy, S. Karna, P. M. Ajayan, R. Vajtai, *Nano Lett.,* 2012, **12,** 5616-5621.

49 J. R. McDonough, J. W. Choi, Y. Yang, F. L. Mantia, Y. Zhang, Y. Cui, *Appl. Phys. Lett.,* 2009, **95,** 243109-243103.

50 F. H. Meng, Y. Ding, *Adv. Mater.,* 2011, **23,** 4098-4102.

51 K. H. Kim, M. Yang, K. M. Cho, Y. S. Jun, S. B. Lee, H. T. Jung, *Scientific Report,* 2013, **3,** 3251-3259.

52 J. Zang, X. Li, *J. Mater. Chem.,* 2011, **21,** 10965-10969.

53 X. Ding, Y. Zhao, C. Hu, Y. Hu, Z. Dong, N. Chen, Z. Zhang, L. Qu, *J. Mat. Chem. A*, 2014, 2, 12355-12360.

54 V. T. Le, H. Kim, A. Ghosh, J. Kim, J. Chang, Q. A. Vu, D. T. Pham, J. H. Lee, S. W. Kim, Y. H. Lee, *ACS Nano*, 2013, **7,** 5940-5947.

55 Y. Fu, X. Cai, H. Wu, Z. Lv, S. Hou, M. Peng, X. Yu, D. Zou, *Adv. Mater.,* 2012, **24,** 5713-5718.

56 J. Ren, W. Bai, G. Guan, Y. Zhang, H. Peng, *Adv. Mater.*, 2013, **25,** 5965-5970.

57 J. Bae, M. K. Song, Y. J. Park, J. M. Kim, M. Liu, Z. L. Wang, *Angew. Chem. Int. Ed.,* 2011, **50,** 1683-1687.

Table 1. Preparation conditions of MWCNT assisted PANI samples and their area specific capacitance.

Sample ID	**Volume (mL) of MWCNT in 50 mL of 0.12 mol L^{-1} aniline solution (in 1 mol L^{-1} H_2SO_4)**	**Specific capacitance mF/cm^2 at 0.1 mA in 1 mol L^{-1} $TEABF_4$ measured in three-electrode cell**
PANI	0	48.3
MWCNT-PANI-a	0.5	53.4
MWCNT-PANI-b	1.0	63.9
MWCNT-PANI-c	2.0	85.8
MWCNT-PANI-d	3.0	57.6

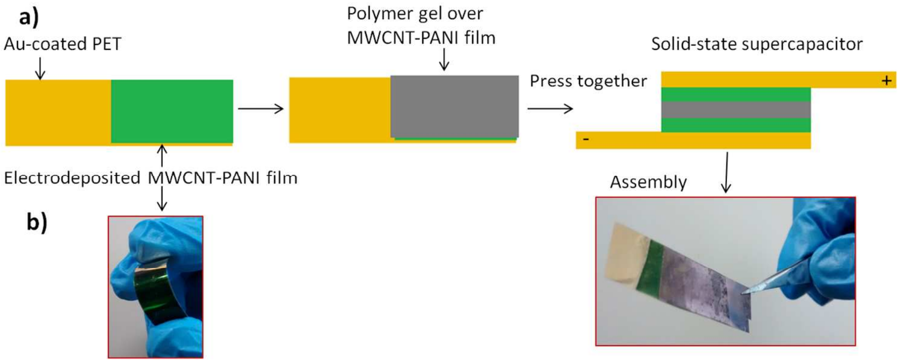

Fig. 1 a) schematic illustration of the fabrication process of flexible solid-state supercapacitor and (b) digital photographs of electrodeposited film and solid-state assembly.

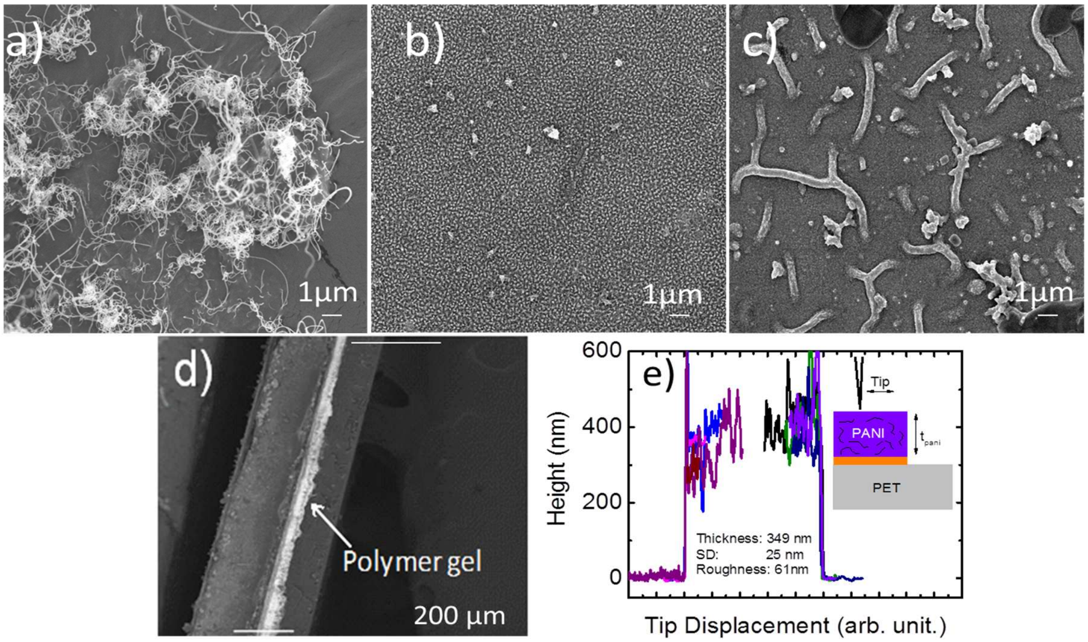

Fig. 2 SEM images of a) MWCNT, b) Pure PANI film, c) MWCNT-PANI film, and d) Cross section view of sandwich assembly of solidified two electrodes with polymer gel electrolyte, and e) Graph shows the profilometer operation on MWCNT-PANI film at different regions.

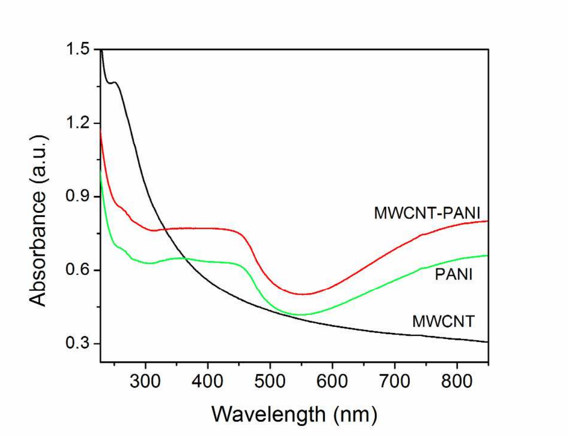

Fig. 3 UV-vis spectra of MWCNT-PANI, pure PANI, and MWCNT.

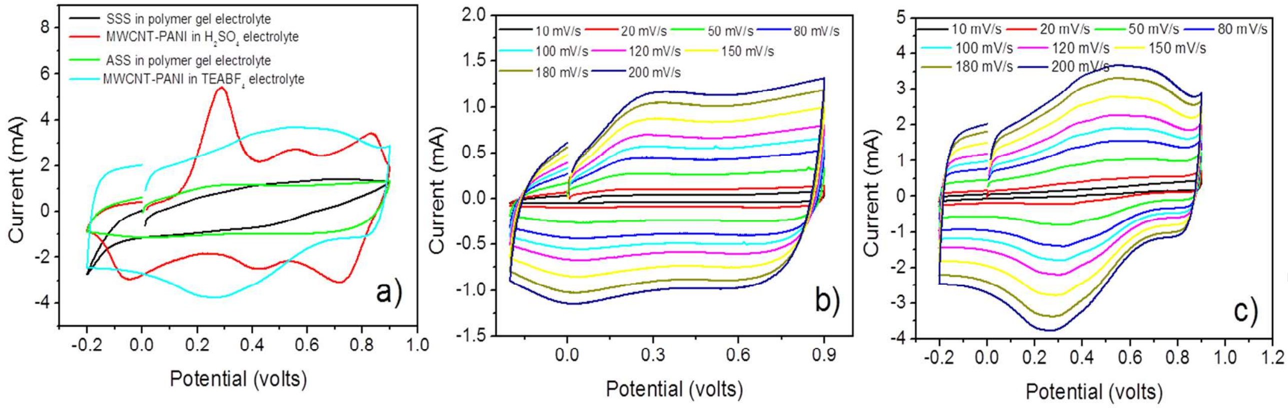

Fig. 4 a) CV curves of MWCNT-PANI-c with different electrolytes at 200 mV/s, b) CV curves of MWCNT-PANI-c with gel electrolyte at different scan rates, and c) CV curves of MWCNT-PANI-c with organic electrolyte at different scan rates.

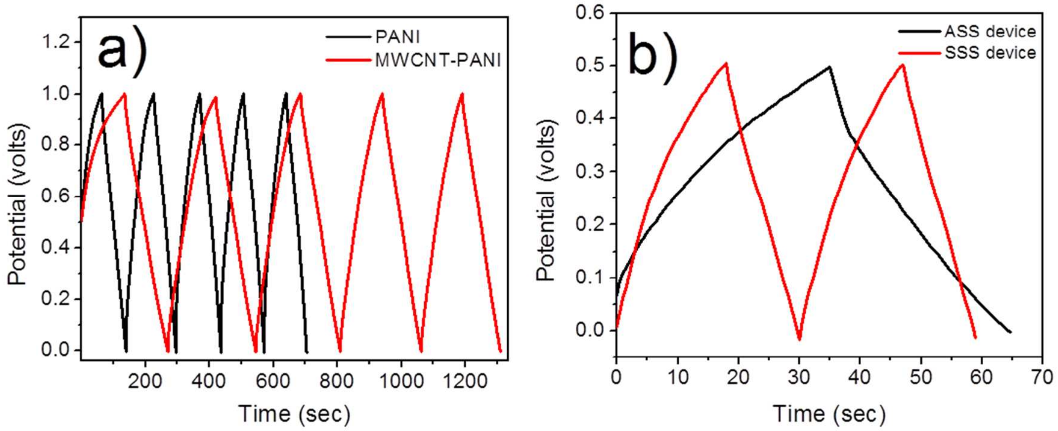

Fig. 5 a) Galvanostatic charge discharge curves of pure PANI and MWCNT-PANI-c in 1 mol L^{-1} $TEABF_4$ electrolyte, and b) Galvanostatic charge discharge curves of SSS and ASS measured in full cell configuration with H_3PO_4-PVA gel electrolyte.

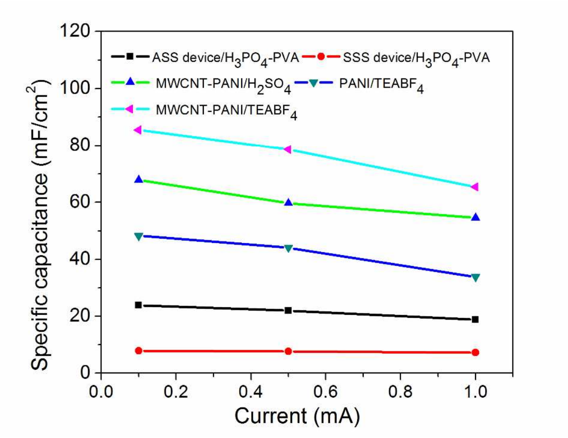

Fig. 6 Area-specific capacitance of MWCNT-PANI-c and pure PANI with different electrolytes.

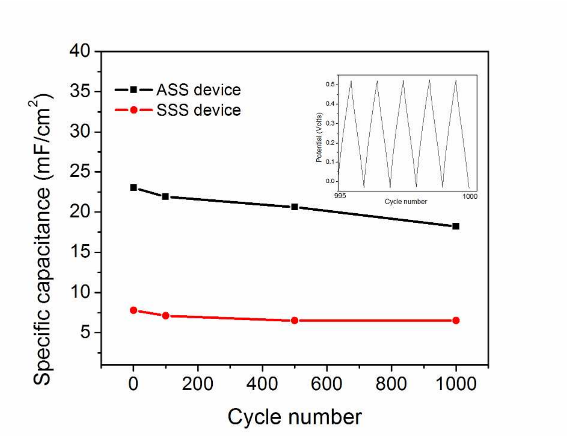

Fig. 7 Cyclic performance of SSS and ASS devices. The inset represents the galvanostatic charge-discharge curves after 1000 cycles of SSS device.

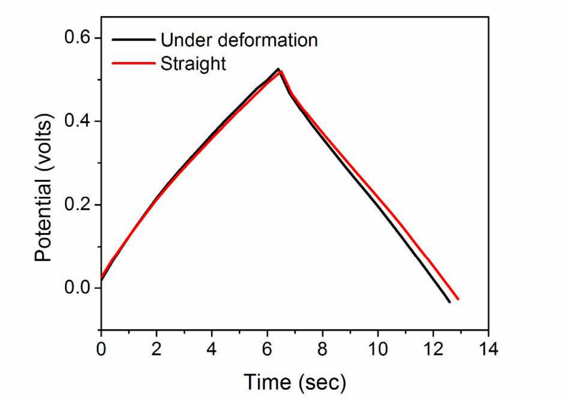

Fig. **8** Galvanostatic charge discharge curves of SSS device under deformation and straight status.

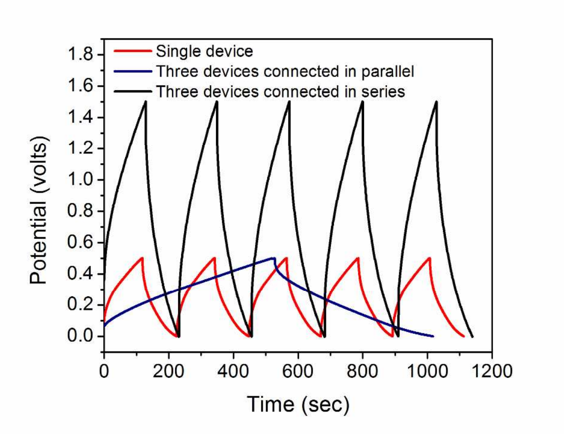

Fig. 9 Galvanostatic charge discharge curves of single ASS device, three ASS devices in series, and three ASS devices in parallel forms.